Numerical Methods in Laminar and Turbulent Flow

Volume VII, Part 2

Editors:
C. TAYLOR
J. H. CHIN
G. M. HOMSY

Proceedings of the Seventh International Conference held in Stanford, 15th–19th July, 1991

Calculation of the Flow Around a High-Lift Airfoil Using an Explicit Code and an Algebraic Reynolds Stress Model

L. Davidson

CERFACS (*European Centre for Research and Advanced Training in Scientific Computation*) 42, Avenue G. Coriolis, 31057 Toulouse, FRANCE [1]

ABSTRACT

In the Computational Aerodynamic Team at **CERFACS** work is going on calculating the flow around low-speed high-lift two-dimensional airfoils ($R_e = 2.1 \times 10^6$; $M = 0.15$) with the object to be able to predict stall. Work has been carried out improving the numerical scheme [1], as well as implementing and testing different turbulence models, such as the Baldwin-Lomax model and various $k - \varepsilon$ models [2,3]. The main problem in these works was that the separation zone near the trailing edge was much under-predicted compared with experiments, and when the angle of attack was increased the predicted lift coefficient increased even though the experiments show that stall should occur. It was believed that this failure of predicting stall could be due to inadequate turbulence models.

The turbulence on the suction surface of the profile is affected by the wall curvature and streamline curvature; near and in the separation region, the streamwise normal Reynolds stress is much larger than that transversal one. None of the turbulence models tested so far can model these important phenomena, but over-predict the Reynolds stresses in the shear layer, and, consequently, predict the separation point too late and the separation zone much too small. This paper treats calculation of the flow described above using an explicit, compressible, time-marching code and an Algebraic Reynolds Stress Model (ASM); this model has the ability to account for curvature effects on the turbulence, as well as for the strong non-isotropy of the turbulence.

1 THE CODE

The code, which is based on that by Rizzi & Müller [4], solves the continuity equation ρ, the momentum equations $\rho u, \rho v$, and the equation for total energy

[1] Present adress: Department of Thermo and Fluid Dynamics, Chalmers University of Technology, S-412 96 Gothenburg, SWEDEN

ρe_o; the pressure is calculated using the gas law. The main features of the code are:

- explicit, compressible time-marching, cell-centered finite volume, central differencing, local time stepping
- four stage Runge-Kutta scheme for the mean flow equations
- the k and ε equations are solved using a semi-implicit solver (hybrid central/upwind scheme, ADI) [2]
- fourth-order numerical non-homogenous dissipation term in all mean flow equations [5]

Initially, attempts were carried out to solve the k and ε equations explicitly using the existing Runge-Kutta solver. However, no stable, convergent solution was obtained. The main cause for these problems was probably the large source terms. These terms contain the ratio ε/k which in regions of weak turbulence (laminar regions) causes problems since both k and ε tend to zero. In order to remedy these stability problems a semi-implicit solver was implemented for solving k and ε [2].

2 THE TURBULENCE MODEL

2.1 The Algebraic Stress Model

The algebraic Reynolds stress model is a standard one, which – using Cartesian velocity components – reads [6]

$$\overline{u_i u_j} = \frac{2}{3}\delta_{ij}k + \frac{k}{\varepsilon}\frac{(1-c_2)(P_{ij} - \frac{2}{3}\delta_{ij}P_k) + \Phi'_{ij,1} + \Phi'_{ij,2}}{c_1 + P/\varepsilon - 1} \qquad (1)$$

where the standard modelization of the pressure-strain correlation terms [6] have been used, and where the near-wall correction terms and the production term have the form

$$\begin{aligned}
\Phi'_{ij,1} &= c'_1\frac{\varepsilon}{k}(\overline{u_n^2}\delta_{ij} - \frac{3}{2}\overline{u_n u_i}\delta_{nj} - \frac{3}{2}\overline{u_n u_j}\delta_{ni})f(\frac{\ell_t}{x_n}) \\
\Phi'_{ij,2} &= c'_2(\Phi_{nn,2}\delta_{ij} - \frac{3}{2}\Phi_{ni,2}\delta_{nj} - \frac{3}{2}\Phi_{nj,2}\delta_{ni})f(\frac{\ell_t}{x_n}) \\
P_{ij} &= -\overline{u_i u_k}\frac{\partial U_j}{\partial x_k} - \overline{u_j u_k}\frac{\partial U_i}{\partial x_k}
\end{aligned}$$

The f-function is a damping function which reduces the effect of the wall correction with increasing distance x_n (n denotes normal direction), and which has the form $f = k^{3/2}/(2.55x_n\varepsilon)$. The constants are standard ones [6]: $c_1 = 1.8$, $c'_1 = 0.5$, $c_2 = 0.6$, $c'_2 = 0.3$.

Note that the near-wall correction terms are in simplified form, which is based on the assumption that the walls are parallel to the Cartesian velocity

components. This assumption seems to be reasonable, see Fig. 1. However, tests were also carried out using the general formulation [7], and it was found that the contribution from $\overline{u^2}$ in the expression for $\Phi'_{12,1}$ gave a large amplifying effect, which almost cancelled the damping effect due to the $\overline{uv}$-term. The wall correction term $\Phi'_{12,1}$ has the form

$$\Phi'_{12,1} = -c'_1 \frac{\varepsilon}{k} \frac{3}{2} [\overline{uv} + (\overline{u^2} + \overline{v^2}) n_x n_y] f(\frac{\ell_t}{x_n})$$

and it becomes almost zero on the suction side near the trailing edge (in the separation region). This is due to that the product $n_x n_y$ is not negligible (up to 0.2), and that the normal stress $\overline{u^2}$ is much larger than the shear stress. For these reasons the simplified formulation, which does damp the shear stress in the separation region, was used.

The Reynolds stresses are stored at the cell centres. This is contrary to what is normally done in implicit codes based on SIMPLE-methods [8], where the shear stresses are staggered and stored on the faces of the control volumes of the velocities in order to enhance stability. In this work the solution procedure was found to be stable without staggering the shear stresses; this is probably because the mean flow variables are solved *explicitly*, which means that all terms are at the right-hand-side of the discretized equations, and thus the solution procedure is less sensitive to the explicit adding of the Reynolds stresses than the SIMPLE-methods. For more details on the implementation of the ASM, see [9].

2.2 The k and ε Equations

Since k and ε appear in the equation for the Reynolds stresses $\overline{u_i u_j}$ in Eq. 1, the equations for k and ε have also to be solved. The standard modellized k and ε-equations in the ASM have the form:

$$\begin{aligned}
\frac{\partial}{\partial x_j}(\rho U_j k) &= \frac{\partial}{\partial x_j}[(\mu + c_k \rho \overline{u_j u_m} \frac{k}{\varepsilon}) \frac{\partial k}{\partial x_m}] + P_k - \rho\varepsilon \\
\frac{\partial}{\partial x_j}(\rho U_j \varepsilon) &= \frac{\partial}{\partial x_j}[(\mu + c_\varepsilon \rho \overline{u_j u_m} \frac{k}{\varepsilon} \frac{\partial \varepsilon}{\partial x_m}] + \frac{\varepsilon}{k}(c_{1\varepsilon} P_k - c_{2\varepsilon} \rho\varepsilon) \\
P_k &= -\rho \overline{u_i u_j} \frac{\partial U_i}{\partial x_j}, \quad c_k = 0.22,\ c_\varepsilon = 0.17,\ c_{1\varepsilon} = 1.44,\ c_{2\varepsilon} = 1.92
\end{aligned}$$

Normally the diffusion terms in the k and ε-equations have little influence on the flow field. Calculations modelling these diffusion terms using the eddy viscosity assumption were also carried out, but no noticeable changes in the calulated results were observed.

The k and ε-equations are solved implicitly, which considerably enhances the stability [2]. This solution method is used in codes based on SIMPLE-methods [10]. The main characteristics are hybrid central/upwind differencing, and Three-Diagonal-Matrix-Algorithm for solving the discretized linear equations in both coordinate directions.

2.3 Near-Wall Treatment

Near the walls the one-equation model by Wolfshtein [11], modified by Chen and Patel [12], is used. In this model the standard k equation is solved; the diffusion term in the k-equation is modelled using the eddy viscosity assumption. The turbulent length scales are prescribed as:

$$\ell_\mu = c_\ell n[1 - exp(-R_n/A_\mu)], \quad \ell_\varepsilon = c_\ell n[1 - exp(-R_n/A_\varepsilon)]$$

(n is the normal distance from the wall) so that the dissipation term in the k-equation and the turbulent viscosity are obtained as:

$$\varepsilon = \frac{k^{3/2}}{\ell_\varepsilon}, \quad \mu_t = c_\mu \sqrt{k} \ell_\mu \tag{2}$$

The Reynolds number R_n and the constants are defined as

$$R_n = \frac{\sqrt{k}n}{\nu}, \; c_\mu = 0.09, \; c_\ell = \kappa c_\mu^{-3/4}, \; A_\mu = 70, \; A_\varepsilon = 2c_\ell$$

The one-equation model is used near the walls (for $R_n \leq 250$; the matching line is chosen along a pre-selected grid line), and the standard k and ε-equations in the remaining part of the flow. Since the ASM is not valid near the wall, the Reynolds stresses are here computed using the Boussinesq assumption, i.e.

$$\rho \overline{u_i u_j} = -\mu_t \left(\frac{\partial U_i}{\partial x_j} + \frac{\partial U_j}{\partial x_i} - \frac{2}{3} \delta_{ij} \frac{\partial U_m}{\partial x_m} \right) + \frac{2}{3} \delta_{ij} \rho k \tag{3}$$

where μ_t is calculated using Eq. 2. The matching of the one-equation model and the k and ε-equations does not pose any problems but gives a smooth distribution of μ_t and ε across the matching line. However, the matching of the ASM and the one-equation model gives rise to non-continuity in the Reynolds stresses across the matching line. The one-equation model gives more or less isotropic normal Reynolds stresses according to Eq. 3, whereas ASM gives highly non-isotropic Reynolds stresses, which results in a jump in the profiles of $\overline{u^2}$ and $\overline{v^2}$ across the matching line. Also the $\overline{uv}$-profile is non-smooth across the matching line due to an inconsistency between the one-equation model (or the $k - \varepsilon$ model) and the ASM. In order to illustrate this, a boundary layer flow is chosen where the only important velocity gradient is $\partial U/\partial y$, and where

$$f = 1, \; P_k \simeq \varepsilon, \; P_k = -\overline{uv} \frac{\partial U}{\partial y}$$

so that Eq. 1 gives

$$\overline{v^2} = \frac{2}{3} k \frac{c_1 - 1 + c_2(1 - 2c_2')}{c_1 + 2c_1'}, \quad -\overline{uv} = \frac{1 - c_2 + \frac{3}{2} c_2 c_2'}{c_1 + \frac{3}{2} c_1'} \overline{v^2} \, \frac{k}{\varepsilon} \frac{\partial U}{\partial y} \tag{4}$$

Inserting values for the constants gives $-\overline{uv} = 0.065 \, k^2/\varepsilon \, \partial U/\partial y$. The coefficient 0.065 should be compared with $c_\mu = 0.09$ which the $k - \varepsilon$ model as well as the one-equation model gives.

The matching problems discussed above do not seem to create any serious problems: the equations remain stable, despite small jumps in the Reynolds stress profiles.

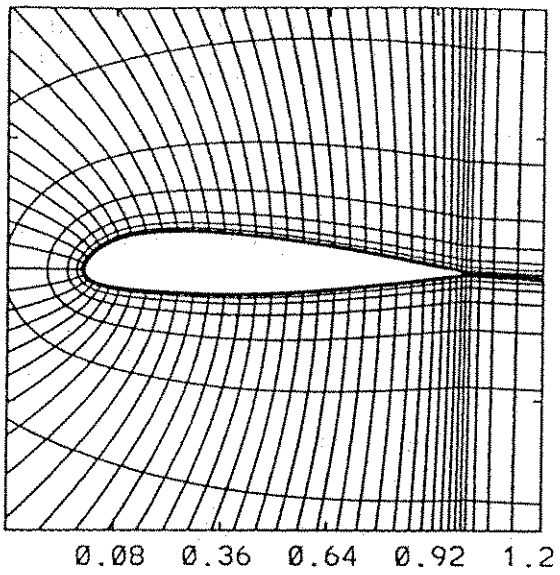

Figure 1. The grid near the profile. (only every 4th grid line is drawn)

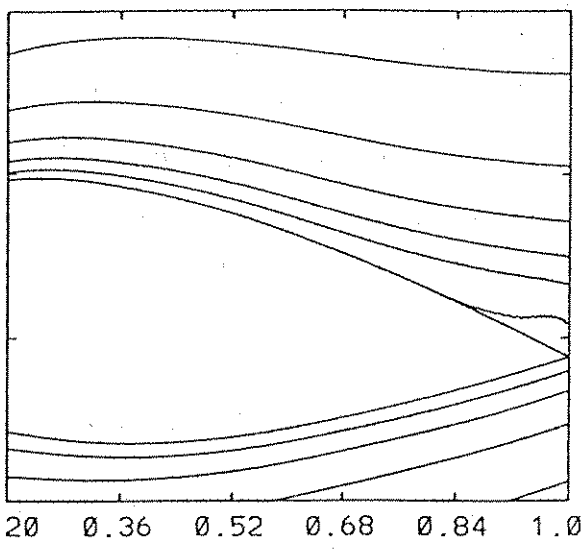

Figure 2. Streamlines near the trailing edge.

3 RESULTS

A C-mesh with 353 × 65, generated by Chanez and Palicot [13], has been used (see Fig. 1). The near-wall nodes are located at $y^+ \simeq 1$, and 7 to 10 nodes – in the normal direction – are situated in the region $0 \leq y^+ \leq 20$.

The calculated results (for more details, see [9]) are compared with experimental data taken from [14,15]. The Reynolds number and the Mach number are 2.1×10^6 and 0.15, respectively. Measurements have been carried out in two windtunnels, F1 and F2. In the F1 windtunnel, global characteristics such as friction coefficients and surface pressures were measured. The flow field was studied more in detail in the F2 windtunnel, where mean velocity profiles and Reynolds stresses were measured using a three component LDV-system. The blockage effect in the F2 tunnel was more important than in the F1 tunnel, leading to three-dimensional effects for $\alpha \geq 13°$.

	F1 Data	F2 Data	ASM
C_L (13.3°)	1.55	1.49	1.53
separation (13.3°)	0.94	-	0.78
C_L (15.3°)	1.65	1.29	1.64
separation (15.3°)	0.82	-	0.68
C_L (16.3°)	1.23	1.25	1.53
separation (16.3°)	-	-	0.54

Table 1: Comparison of calculated global characteristics with experiments.

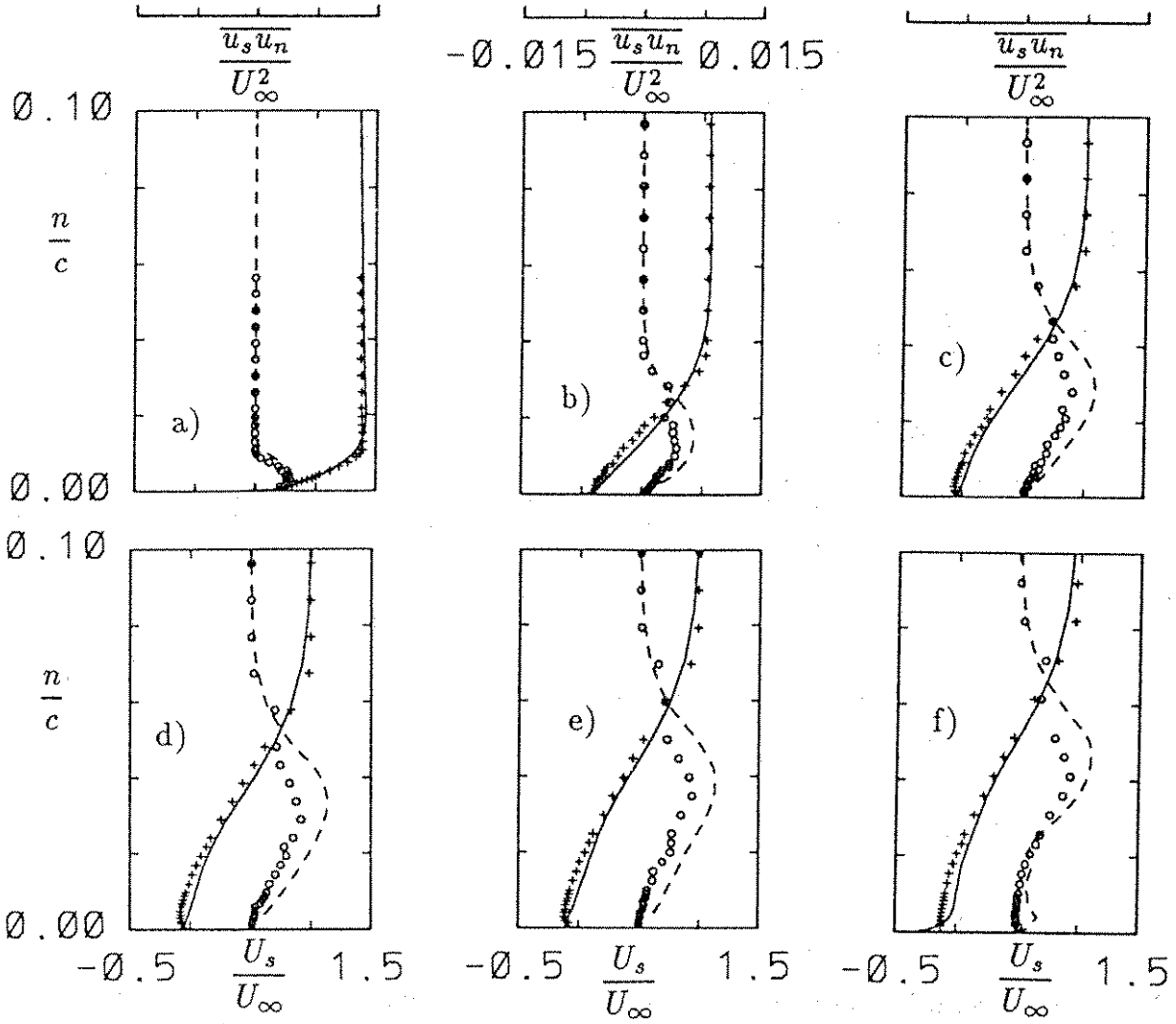

Figure 3: U_s and $-\overline{u_s u_n}$-profiles on the suction side. Solid lines: U_s/U_∞; dashed lines: $-\overline{u_s u_n}/U_\infty^2$; markers: experiments. a) $x/c = 0.4$, b) $x/c = 0.775$, c) $x/c = 0.9$, d) $x/c = 0.93$, e) $x/c = 0.96$, f) $x/c = 0.99$.

The global characteristics are compared with experimental data in Table 1. The ASM gives C_L-values in good agreement with experiments. When α is increased, a decrease in C_L is predicted (i.e. approaching stall) for $\alpha = 16.3°$, which is in agreement with experiments. The point of separation in Table 1 is defined as where the skin-friction changes sign. The ASM seems to predict too large a separation. When the velocity profiles are studied (see below), it will turn out, however, that the separation zone is predicted well in agreement with experiments.

The calculated results are presented below more in detail for $\alpha = 13.3°$. The U_s-velocities and the shear stresses on the suction side of the airfoil are presented in Fig. 3. Note that in Fig. 3 an orthogonal $s - n$ coordinate system is used. The s-coordinate is tangential to the airfoil, with origin on the surface. The U_s-velocities on the profile are well predicted. The somewhat poorer agreement in the U_s-profiles in the outer part of the shear layer may be due to that the mesh is here rather coarse. As separation is approached, it is seen that the predicted U_s-profiles follow the experimental ones, the profiles getting progressively less

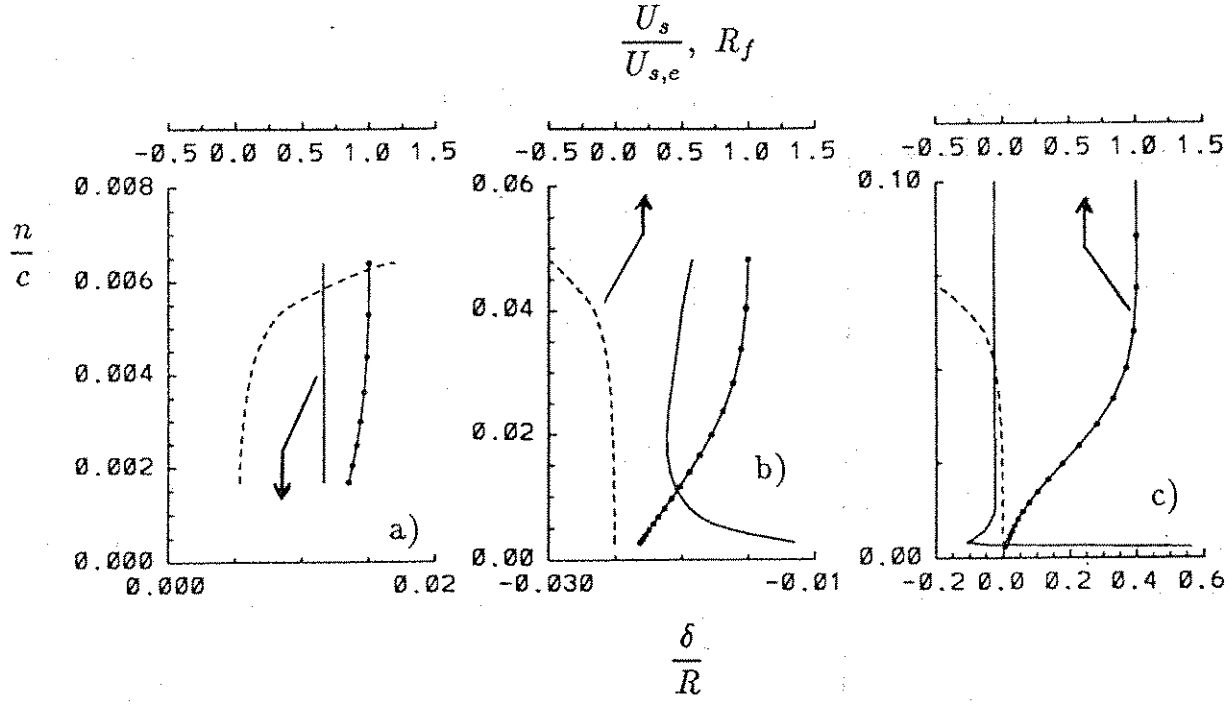

Figure 4: Influence of curvature on the turbulence. Calculations. ———, δ/R; – – – –, R_f; —•—•—, $U_s/U_{s,e}$. a) $x/c = 0.2$, b) $x/c = 0.775$, c) $x/c = 0.9$

full and that an inflextion point in the profiles appears.

3.1 Turbulent Quantities

When the streamlines of the mean flow have a convex curvature (on the suction side for $x/c \leq 0.6$; see Fig. 2) the turbulence is stabilized, which dampens the turbulence [6,16], especially the shear stress and the Reynolds stress normal to the wall. The ratio of boundary layer thickness δ to curvature radius R is a common parameter for quantifying the curvature effects on the turbulence. The work reviewed by Bradshaw [16] demonstrates that even such small amounts of convex curvature as $\delta/R = 0.01$ can have significant effect on the turbulence. Thompson and Whitelaw [17] carried out an experimental investigation on a configuration simulating the flow near a trailing edge of an airfoil, where they measured $\delta/R \simeq 0.03$. They report a 50 percent decrease of $\overline{u_n^2}$ (Reynolds stress in the normal direction to the wall of the airfoil) on the suction side due to curvature. The reduction of $\overline{u_s^2}$ and $-\overline{u_s u_n}$ were also substantial. They also report significant damping of the turbulence in the shear layer in the outer part of the separation region.

Since Cartesian velocity components have been used in the calculations, no explicit curvature terms appear in the Reynolds-stress equations (see Eq. 1). Of course, also the Reynolds stresses formulated in Cartesian coordinates are affected by curvature, but *implicitly*. In order to investigate the curvature effects, let us – in the post-processing – study the equations in polar coordinates $r - \theta$, with the flow in the circumferential θ-direction (i.e. $U_\theta = U_\theta(r), U_r = 0$). The θ-axis is thus chosen so that the flow is *locally* aligned with this axis. Curvature

terms appear now because the $r = const.$-coordinate lines are curved. If the curvature terms due to diffusion are neglected, the Reynolds stress equation can, in symbolic form, be written [18]

$$C_{ij} - D_{ij} = P_{ij} + \Phi_{ij} - \varepsilon_{ij} + P^c_{ij} + C^c_{ij} \tag{5}$$

where superscript c on P_{ij} and C_{ij} denotes curvature terms originating from production and convection, respectively, see Table 2. The larger these terms, the more important the curvature effects.

The flux Richardson number

$$R_f = \frac{2U_\theta/r}{U_\theta/r + \partial U_\theta/\partial r}$$

is a convenient parameter for studying curvature effects. Its physical meaning is (minus) the ratio of the production of $\overline{u_r^2}$ due to curvature, to the total production of $\overline{u_\theta^2}$ (see Table 2). The Reynolds stresses can, using $r-\theta$ coordinates, be expressed as a function of R_f; assuming $f = 0$ Eq. 1 gives

$$\frac{\overline{u_r^2}}{k} = \frac{2}{3}\frac{c_1 - 1 + c_2 P_k/\varepsilon}{c_1 + P_k/\varepsilon - 1} - \frac{2R_f}{1-R_f}\frac{1}{c_1 + P_k/\varepsilon - 1} \tag{6}$$

$$\frac{\overline{u_\theta^2}}{k} = \frac{2}{3}\frac{c_1 - 1 + (3-2c_2)P_k/\varepsilon}{c_1 + P_k/\varepsilon - 1} + \frac{2R_f}{1-R_f}\frac{1}{c_1 + P_k/\varepsilon - 1} \tag{7}$$

$$\overline{u_r u_\theta} = -\frac{(1-c_2)}{c_1 + P_k/\varepsilon - 1}\left[1 - \frac{R_f}{(1-c_2)(2-R_f)}\left(2\frac{\overline{u_\theta^2}}{\overline{u_r^2}} - 1\right)\right]\frac{k}{\varepsilon}\frac{\overline{u_r^2}}{k}\frac{\partial U_\theta}{\partial r} \tag{8}$$

Note that this is not the same expression as derived in [6], since they included the curvature terms C^c_{ij} in P_{ij} when calculating the pressure-strain terms. The ratio δ/R, the flux Richardson number, and the velocity profile (in order to faciliate the identification of the boundary layer) are shown in Fig. 4 at three different x-stations: at $x/c = 0.2$ where the wall curvature is most important, near the separation point ($x/c = 0.775$), and in the separation zone ($x/c = 0.9$). As can be seen the streamline curvature is positive at $x/c = 0.2$ (compare

	P_{ij}	P^c_{ij}	C^c_{ij}
$\overline{u_r^2}$	-	$2\overline{u_r u_\theta}\dfrac{U_\theta}{r}$	$2\overline{u_r u_\theta}\dfrac{U_\theta}{r}$
$\overline{u_\theta^2}$	$-2\overline{u_r u_\theta}\dfrac{\partial U_\theta}{\partial r}$	-	$-2\overline{u_r u_\theta}\dfrac{U_\theta}{r}$
$\overline{u_r u_\theta}$	$-\overline{u_r^2}\dfrac{\partial U_\theta}{\partial r}$	$\overline{u_\theta^2}\dfrac{U_\theta}{r}$	$(\overline{u_\theta^2} - \overline{u_r^2})\dfrac{U_\theta}{r}$

Table 2: Source terms in the Reynolds stress equations (see Eq. 5) due to production and convection in a polar coordinate system

Fig. 2), which in the outer part of the boundary layer gives an increasing flux Richardson number. The curvature effects are largest in the outer boundary layer, where the curvature term U_θ/R becomes comparable with the velocity gradient $\partial U_\theta/\partial r$. The *direct* influence of the curvature effects are thus largest in the outer part of the boundary layer, but they will also have *indirect* influence via the k and ε-equations. The Reynolds stresses, augmented or damped by curvature, increase or decrease the production terms in the k and ε-equations and, through convection and diffusion, also affect the surroundings. As separation is approached the streamlines become concave (see Fig. 2), which destabilizes the turbulence. In Fig. 4 it is seen that δ/R and R_f are negative.

In separated flows the streamlines bounding the separation region are usually convex. It may be noted that in the present case, the turbulence in the shear layer bounding the separation zone on the suction side is mostly destabilized due to the concave curvature of the streamlines; these become convex first when the flow on the suction side reaches the wake.

The last term in square brackets in the equation for the shear stress (Eq. 8) is due to curvature. It expresses the importance of curvature effects on the shear stress; for negligible curvature effects it is zero. At $x/c = 0.2$, where the stabilizing curvature effects are most important, it attains values of approximately 1.5 (in the very outer part of the boundary layer). Further downstream it decreases, and near the separation point it becomes negative because of the destabilizing curvature effects. In the shear layer of the separation region the term reaches values close to -1.5.

In boundary layer flow the only term which contributes to the production term in the k and ε-equations is $-\overline{u_s u_n}\partial U_s/\partial n$. Thompson and Whitelaw [17] found that near the separation point, as well as in the separation zone, the production term $-(\overline{u_s^2} - \overline{u_n^2})\partial U_s/\partial s$ was of equal importance. In Fig. 5 these terms are presented. At $x/c = 0.2$ the production term due to the normal stresses is not very large (at the most, ten percent of that due to the shear stress). Near the separation point and in the separation region, the two terms are of equal importance. In Fig. 5 the dissipation is also presented, and it is seen that production and dissipation balance each other at $x/c = 0.2$, but that near the separation point and especially in the separation region, this is not the case. The production term using the eddy viscosity assumption $\nu_t(\partial U_s/\partial n)^2$ (the contribution from the normal stresses is negligible) is also included in Fig. 5, which should be compared with $-\overline{u_s u_n}\partial U_s/\partial n$. Note that this is a comparison between the shear stress obtained with the ASM, and that obtained using the eddy viscosity assumption $\overline{u_s u_n} = -\nu_t \partial U_s/\partial n$. It can be seen that the shear stress obtained using the eddy viscosity assumption is considerably larger than that obtained using the ASM. This is because the ASM accounts for the damping of the shear stress and the Reynolds stress normal to the wall; for boundary layer flow the ASM yields, with damping, a c_μ-coefficient of 0.065 (see Eq. 4), which is 28 percent smaller than the c_μ used in $k-\varepsilon$ models.

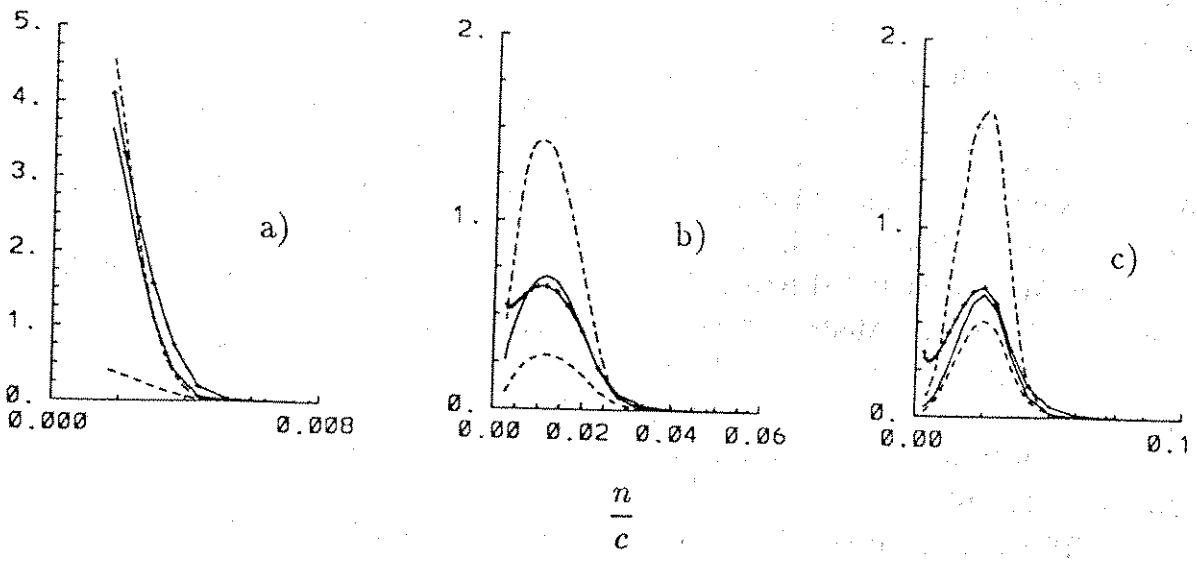

Figure 5: Calculated productions terms in the k-equation.
———, $-\overline{u_s u_n}\partial U_s/\partial n$; – – ––, $(\overline{u_n^2} - \overline{u_s^2})\partial U_s/\partial s$; — – —, $\nu_t[\partial U_s/\partial n]^2$;
—+—+—, ε. a) $x/c = 0.2$, b) $x/c = 0.775$, c) $x/c = 0.9$

4 CONCLUSIONS

The flow around a two-dimensional high-lift airfoil has been calculated using an algebraic stress model. As the ASM is only valid for fully turbulent flow it has been matched with a one-equation model close to the wall ($y^+ \leq 50$). This turbulence model has been shown to be able to predict stall for an angle of attack of 16°, which is in agreement with experiments. Earlier work [2-3] has shown that $k - \varepsilon$ models are not able to predict stall, and that these models over-predict the shear stress, and consequently predicts separation too late and separation regions too small. The main reasons for the superiority of the ASM are believed to be its ability of taking into account the influence of streamline curvature and the large difference in the normal Reynolds stresses.

It was found that the general formulation of the near-wall correction terms in the ASM gave too small damping (or none at all) of the shear stress in the separation region. The simplified form – which assumes walls parallel to the Cartesian velocity components – was used, which gave predicted results better in agreement with experiments. It was found, furthermore, that this damping is very important, and that it contributes to the superiority of the ASM over the $k - \varepsilon$ model.

5 REFERENCES

1. GENDRE, P. - Computation of Low Speed Flow Around High-Lift Single Element

Airfoils With a 2D Navier-Stokes Solver, Proc. Second World Congress on Computational Mechanics, extended abstracts, pp. 202-205, Stuttgart, 1990.
2. DAVIDSON, L. - Implementation of a Semi-Implicit $k-\varepsilon$ Turbulence Model in an Explicit Runge-Kutta Navier-Stokes Code, TR/RF/90/25, CERFACS, 1990.
3. de CAMBRAY, E. - Evaluation d'un modèle $k-\varepsilon$ dans un code Navier-Stokes, Thèse DEA, CERFACS, September, 1990.
4. RIZZI A. and MÜLLER, B. - Large-Scale Viscous Simulation of Laminar Vortex Flow Over a Delta Wing, *AIAA Journal*, **27**, 833-840, 1989.
5. SWANSON, R.C. and TURKEL, E. - Artificial Dissipation and Central Difference Schemes for the Euler and Navier-Stokes Equations, AIAA Paper No 87-1107, 1987.
6. RODI, W. and SCHEUERER, G. - Calculation of Curved Shear Layers With Two-Equation Turbulence Models, *Phys. Fluids*, **26**, No. 6, pp. 1422-1435, 1983.
7. LAUNDER, B.E, REECE, G.J. and RODI, W. - Progress in the Development of a Reynolds-Stress Turbulence Closure, *JFM*, **68**, pp. 537-566, 1975.
8. POPE, S.B. and WHITELAW, J.H. - The Calculation of Near-Wake Flows, *JFM*, **73**, pp. 9-30, 1976.
9. DAVIDSON, L. - Predicting Stall of a Two-Dimensional Airfoil Using an Algebraic Reynolds Stress Turbulence Model, Rept., CERFACS, 1991.
10. PATANKAR, S.V. - Numerical Heat Transfer and Fluid Flow, McGraw-Hill, New York, 1980.
11. WOLFSHTEIN, M. - The Velocity and Temperature Distribution in One-Dimensional Flow with Turbulence Augmentation and Pressure Gradient, *Int. J. Mass Heat Transfer*, **12**, pp. 301-318, 1969.
12. CHEN, H.C. and PATEL, V.C. - Practical Near-Wall Turbulence Models for Complex Flows Including Separation, AIAA Paper No 87-1300, Honolulu, June 1987.
13. CHANEZ, Ph. and PALICOT, L. - Évaluation d'un code Navier-Stokes bidimensionnnel pour le calcul de l'écoulement autour d'un profile d'aile, Note interne Aerospatiale, 443.548/90, 1990
14. CAPBERN, C. and BONNET, C. - Opération décrochage: Rapport Final de Synthèse, Rapport Aerospatiale 443.535./89, Toulouse, 1989.
15. GLEYZES, C. - Opération décrochage: Résultats de la deuxième campagne d'essais à F2 (mesures de pression et vélocimetrie laser), Rapport Final ONERA/CERT 57/5004.22, Toulouse, 1989.
16. BRADSHAW, P. - Effects of Streamline Curvature on Turbulent Flow, *AGARDograph*, no. 169, 1973
17. THOMPSON, B.E. and WHITELAW, J.H. - Characteristics of a Trailing-Edge Flow With Turbulent Boundary-Layer Separation, *JFM*, **157**, pp. 305-326, 1985.
18. EKANDER, H. and JOHANSSON, A.V. - An Improved Algebraic Reynolds Stress Model and Application to Curved and Rotating Flows, Proc. 7th Symposium on Turbulent Shear Flows, pp. 21.2.1 - 21.2.6, Stanford, 1989.